Atom-ion quantum gate

Hauke Doerk,[1,2] Zbigniew Idziaszek,[3] and Tommaso Calarco[1,4]
[1]*University of Ulm, Albert-Einstein-Allee 11, D-89069 Ulm, Germany*
[2]*Max-Planck-Institut für Plasmaphysik, Boltzmannstrasse 2, D-85748 Garching, Germany*
[3]*Institute of Theoretical Physics, Faculty of Physics, University of Warsaw, Hoża 69, PL-00-681 Warsaw, Poland*
[4]*ECT, I-38050 Villazzano (TN), Italy*
(Received 22 June 2009; published 26 January 2010)

Ultracold collisions of ions with neutral atoms in traps are studied. Recently, ultracold atom-ion systems have become available in experimental setups, where their quantum states can be coherently controlled. This control allows for an implementation of quantum information processing, combining the advantages of charged and neutral particles. The state-dependent dynamics that is a necessary ingredient for quantum computation schemes is provided in this case by the short-range interaction forces that depend on the hyperfine states of both particles. In this work, a theoretical description of spin-state-dependent trapped atom-ion collisions is developed in the framework of a multichannel quantum-defect theory and an effective single-channel model is formulated that reduces the complexity of the problem. Based on this description, a two-qubit phase gate between a $^{135}Ba^{+}$ ion and a ^{87}Rb atom is simulated using a realistic combination of the singlet and triplet scattering lengths. The gate process is optimized and accelerated with the help of optimal control techniques. The result is a gate fidelity of $1-10^{-3}$ within 350 μs.

DOI: 10.1103/PhysRevA.81.012708 PACS number(s): 34.50.Cx, 37.90.+j, 03.67.Bg, 03.67.Lx

I. INTRODUCTION

Ongoing developments in quantum information processing stimulate an intense search for physical systems suitable for its implementation. Besides solid-state and photonic systems, cold ions and neutral atoms are major candidates in this direction.

Neutral atoms can be accurately manipulated in dipole traps [1,2], optical lattices [3], or on atom chips [4,5]. Advanced evaporative and laser-cooling techniques allow neutral atoms to be prepared in the vibrational ground state of different trapping potentials. Single ions can be confined in Paul or Penning traps [6] and sideband laser cooling allows them to be cooled to the trap ground state.

Ultracold systems that combine ions and neutral atoms are currently being explored [7–9]. Besides several quantum-mechanical aspects of this system, the studies are motivated by the potential applications. For example, techniques involving the sympathetic cooling of trapped atoms by laser-cooled trapped ions can be developed [10,11]. In this paper, we propose a scheme for a quantum gate that combines the advantages of atoms and ions for quantum computation.

The trapping potentials of atoms and ions, although both are made up of oscillating electromagnetic fields, do not interfere with each other since the oscillation frequencies of the respective fields typically differ by orders of magnitude. The strength of the effective ion potential can be much stronger than that for neutral atoms. Tight confinement enables fast transport and, combined with the good addressability of single trapped ions with lasers, this is among the advantages of using ions for implementing quantum computation.

Realization of the Mott insulator phase allows an array of atoms to be prepared with a well-controlled number of particles in a single site of an optical lattice.

Controlled preparation combined with the long decoherence times of neutral atoms is a reason to use atoms for the storage of quantum information. Furthermore, the two-particle interaction between an atom and an ion is typically much stronger than for two neutral atoms, which allows fast gate operations.

While qubits can be stored in internal electronic degrees of freedom for both kinds of particles, the state-dependent dynamics suitable for two-qubit gates requires some engineering of the two-particle interaction. To this end one can use external electromagnetic fields (e.g., magnetic Feshbach resonances), which allow for a precise tuning of the two-body effective scattering properties. The long-range part of the atom-ion interaction also supports a trap-induced type of resonance [12]; because of their generally state-dependent nature, they constitute a basic element of our quantum computation scheme.

This work solely makes use of these trap-induced shape resonances that occur at relatively large distances. In this way, some possible unwanted processes are avoided that may result from molecular dynamics at short distances. We nevertheless plan to include magnetic Feshbach resonances in our theory, which can be applied to perform two-qubit operations in a controlled collision [13,14].

A possible setup for quantum computation is schematically depicted in Fig. 1. Atoms are stored in an optical lattice in a Mott insulator phase such that each lattice site is occupied by exactly one atom. One movable ion is used to create long-distance entanglement between pairs of atoms and to perform quantum gates. The basic ingredient of this idea is the controlled and qubit-sensitive interaction between atoms and ions. In this paper we focus on the dynamics of a single atom interacting with a single ion; nevertheless, our approach can be easily extended to the situation of many atoms, or more than one ion, at a later stage.

In this work we develop a theoretical model for spin-dependent atom-ion collisions. For the case of an alkaline-earth metal ion and an alkali metal atom, a model is formulated based

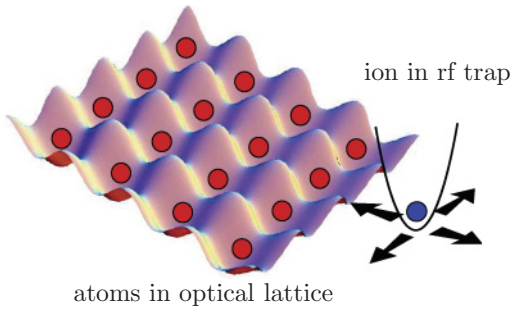

FIG. 1. (Color online) Concept for quantum computation with atoms and ions: Atoms are prepared in an optical lattice in a Mott insulator phase. A movable ion entangles the atoms and can also be used for sympathetic cooling.

on the multichannel quantum-defect theory (MQDT) [9], taking into account the presence of trapping potentials [15]. Within the model, the atom-ion interaction is described by the long-range $1/r^4$ polarization potential combined with a set of quantum-defect parameters representing the effect of the short-range potential. The essential parameters for our approach are the singlet and triplet scattering lengths, which are not yet known with sufficient accuracy but can probably be measured in upcoming experiments. This paper discusses several different regimes for the values of the singlet and the triplet scattering length. For some specific range of scattering lengths, the complexity of the problem can be reduced by employing an effective single-channel model for the atom-ion dynamics.

Using the effective single-channel description, we are able to simulate a two-qubit phase gate for an arbitrary combination of atom and ion species. Applicability of the model, however, requires values of singlet and triplet scattering lengths that are nearly equal. In this case, within the single-channel description and for a specific system of $^{135}Ba^+$ ion and ^{87}Rb atom, we develop a phase-gate process yielding a fidelity of $1-10^{-3}$ within the gate time of 346 μs. Because it is equivalent to the controlled-NOT (CNOT) gate, the phase gate is universal for quantum computation [16]. Therefore, we demonstrate the feasibility of quantum computation on the system under consideration. In a general situation, when the scattering lengths are not similar, the phase gate can be even faster; however, this situation requires going beyond the single-channel effective description and is outside the scope of the present paper.

There are two main mechanisms that could lead to failure of the quantum gate. One is the radiative charge transfer, which in the current scheme leads to a loss of both particles in the case of heteronuclear species. In contrast, for a homonuclear collision [8], the charge transfer results in a physically equivalent situation and therefore cannot be considered a loss mechanism. Heteronuclear alkaline-earth metal ion–alkali metal atom systems have the advantage of a relatively simple electronic level structure; for the systems studied thus far, Na-Ca^+ [9,11] and Rb-Ba^+ [17], the charge exchange rate remains much smaller than the elastic collision rate, even in the presence of resonances. The second type of loss results from spin-changing collisions. In our scheme the qubits are encoded in hyperfine spin states, and collisions leading to final states outside of the computational basis must be avoided. In the regime of applicability of our single-channel effective model, the coupling between different channels is by definition very weak and those kinds of losses can be safely neglected. Even in a general situation, a multichannel treatment including all possible spin-state channels offers the possibility of gaining control over spin-changing processes by appropriate engineering of the gate dynamics.

The paper is organized as follows. Section II describes the basic setup and model used throughout the paper. The atom-ion polarization interaction is discussed briefly and the concepts of correlation diagrams and trap-induced resonances are introduced. The MQDT for trapped particles, as well as its reduction to a single-channel model, is developed in Sec. III. The presented theory allows for the computation of eigenstates and eigenenergies in either single- or multichannel situations. The dynamics of atom-ion collisions is discussed in Sec. IV, where correlation diagrams and the Landau-Zener theory help to understand the features of the system. Section V presents the concepts and results of the two-qubit phase gate simulations. A summary of the results, together with further perspectives and ideas, is given in Sec. VI.

II. BASIC SETUP AND MODEL

We consider a system consisting of a single atom and a single ion, stored in their respective trapping potentials. Such potentials can be created with rapidly oscillating (rf) electric fields for ions and with optical traps based on the ac Stark effect for atoms. These traps can be well approximated as effective time-independent harmonic traps, as long as the particles are close to the ground state of the potential. For this setup we introduce an effective Hamiltonian

$$H = -\frac{\hbar^2}{2m_i}\Delta_i - \frac{\hbar^2}{2m_a}\Delta_a + \frac{1}{2}m_i\omega_i^2(\mathbf{r}_i - \mathbf{d}_i)^2 + \frac{1}{2}m_a\omega_a^2(\mathbf{r}_a - \mathbf{d}_a)^2 + W(|\mathbf{r}_i - \mathbf{r}_a|), \quad (1)$$

where $m_{i(a)}$ is the mass of the ion (atom), $\omega_{i(a)}$ and $\mathbf{d}_{i(a)}$ denote frequency and location of the harmonic trapping potential of the ion (atom), and $W(r)$ is the interaction potential. A microscopic derivation of the Hamiltonian Eq. (1) can be found in Ref. [12]. Here, for simplicity, we have assumed spherically symmetric trapping potentials and the same trapping frequencies for atom and ion: $\omega_i = \omega_a = \omega$. It should be stressed, however, that this approach can be easily generalized to anisotropic trapping potentials and different trapping frequencies [12]. A general treatment would imply coupled c.m. and relative degrees of freedom and, thus, a six-dimensional equation, but there are no fundamental difficulties. In experiments, both traps can be designed to be spherically symmetric, while the assumption of the same trapping frequencies allows us to decouple the relative and c.m. motions, thereby reducing the dimensionality of the problem from six to three. This choice simplifies our numerical calculations, but also allows the most important features of the system to be captured.

We transform the Hamiltonian Eq. (1) by introducing c.m. and relative coordinates, $\mathbf{R}_{\text{c.m.}} = (m_i\mathbf{r}_i + m_a\mathbf{r}_a)/(m_i + m_a)$ and $\mathbf{r} = \mathbf{r}_i - \mathbf{r}_a$, respectively. Without losing generality we

can choose the coordinate frame such that the vector of trap separation, $\mathbf{d} = \mathbf{d}_i - \mathbf{d}_a = d\mathbf{e}_z$, points in the z direction. In this way we obtain the relative Hamiltonian

$$H_{\rm rel}^{(d)} = H_{\rm rel}^{(0)} + \tfrac{1}{2}\mu\omega^2 d^2 - \mu\omega^2 d z, \tag{2}$$

where $\mu = m_i m_a/(m_i + m_a)$ denotes the reduced mass of the atom-ion system and

$$H_{\rm rel}^{(0)} = -\frac{\hbar^2}{2\mu}\Delta_r + \frac{1}{2}\mu\omega^2 r^2 + W(r) \tag{3}$$

is the Hamiltonian for the special case $d = 0$.

A. Atom-ion interaction

At large distances the atom-ion interaction potential has the asymptotic behavior $W(r) \simeq -C_4/r^4$ $(r \to \infty)$. This behavior results from the fact that the ion charge polarizes the electron cloud of the atom, and the induced dipole and the ion attract each other. Therefore, the atom-ion interaction falls into an intermediate category between the long-range Coulomb forces $W(r) \sim 1/r$ and the van der Waals forces $W(r) \sim 1/r^6$ for neutral atoms. The interaction constant C_4 can be expressed in terms of the electric dipole polarizability, α, of the atom in the electronic ground state (S-state): $C_4 = \alpha e^2/2$. The electron charge is denoted as e. At short distances the interaction is dominated by the exchange forces, and higher order dispersion terms (C_6/r^6, C_8/r^8) also become relevant. In the current approach, we model the short-range part of the potential using the quantum-defect method; that is, we do not require the knowledge of the exact form of the short-range interaction. The interaction potential, in addition to the model potential, is depicted schematically in Fig. 2.

By equating the interaction potential C_4/R^{*4} to the kinetic energy $\hbar^2/2\mu R^{*2}$, we can define some characteristic range $R^* = \sqrt{2\mu C_4/\hbar^2}$ and corresponding characteristic energy $E^* = \hbar^2/2\mu R^{*2}$ of the atom-ion interaction. Table I gives the characteristic range and energy for some example atom-ion systems. For comparison, it also includes the harmonic oscillator length $l_0 = \sqrt{\hbar/\mu\omega}$ for $\omega_i = \omega_a = 2\pi \times 100$ kHz.

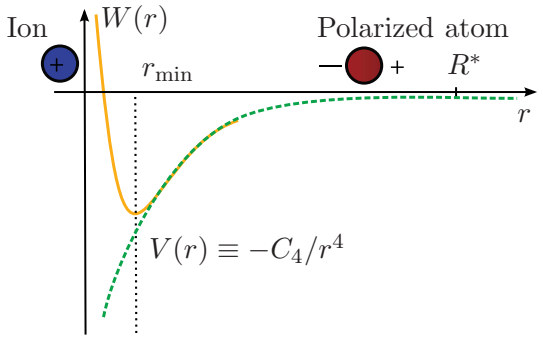

FIG. 2. (Color online) The long-range part of the atom-ion interaction potential equals $-C_4/r^4$. At distances smaller than the potential minimum $r_{\rm min}$, repulsive terms start to dominate. Quantum defect theory replaces the actual potential $W(r)$ (solid line) with a reference potential $V(r)$ (dashed line) and includes the short-range effects using a quantum-defect parameter related to the short-range phase of the relative wave function. The characteristic range R^* of the interaction is typically much larger than $r_{\rm min}$.

TABLE I. Characteristic length and energy scale for example systems. Oscillator lengths are calculated with $\omega_i = \omega_a = 2\pi \times 100$ kHz.

Atom-ion system	R^* (units of a_0)	l_0 (units of a_0)	E^*/h (kHz)
$^{135}Ba^+ + {}^{87}Rb$	5544	826	1.111
$^{40}Ca^+ + {}^{87}Rb$	3989	1178	4.142
$^{40}Ca^+ + {}^{23}Na$	2081	1572	28.545

B. Single-channel quantum-defect treatment

The short-range interaction potential between atom and ion is typically quite complicated and in most cases it is not known theoretically with an accuracy sufficient to determine the scattering properties in the limit of ultracold energies. In order to avoid complications while using the explicit form of the short-range potentials, we resort to the quantum-defect method, which allows the effects of the short-range forces to be included in an effective way. This method consists of substituting the actual potential with the reference potential $V(r) = -C_4/r^4$ at all distances (see Fig. 2) and assigning an appropriate short-range phase to the wave function to model the effects of the short-range potential.

This approach can be illustrated by solving the relative Schrödinger equation $H_{\rm rel}^{(0)}\Psi(\mathbf{r}) = E\Psi(\mathbf{r})$ at $d = 0$. To this end, we apply the partial wave decomposition

$$\Psi(\mathbf{r}) = \sum_{lm} Y_{lm}(\hat{\mathbf{r}})\psi_l(r)/r \tag{4}$$

to obtain the radial Schrödinger equation

$$\left[-\frac{\hbar^2}{2\mu}\frac{\partial^2}{\partial r^2} + \frac{\hbar^2}{2\mu}\frac{l(l+1)}{r^2} + \frac{\mu\omega^2}{2}r^2 + V(r) - E\right]\psi_l(r) = 0 \tag{5}$$

for the radial wave functions $\psi_l(r)$. Here, Y_{lm} are the spherical harmonic functions describing the angular part of the three-dimensional wave function, where l and m are the quantum numbers of the relative angular momentum and its projection on the symmetry axis z, respectively. In the limit of $r \to 0$ we can neglect the trapping potential, energy, and centrifugal barrier in comparison to $V(r) = -C_4/r^4$, which yields

$$\left[-\frac{\hbar^2}{2\mu}\frac{\partial^2}{\partial r^2} - \frac{C_4}{r^4}\right]\psi_l(r) = 0 \tag{6}$$

with the solution

$$\psi_l(r) = r\sin\left(\frac{R^*}{r} + \varphi\right), \quad r \to 0, \tag{7}$$

where φ is a parameter that can be interpreted as the short-range phase. In this method, Eq. (7) is treated as a boundary condition that we impose on the radial wave functions at short distances while solving the relative Schrödinger equation in the general case $d \neq 0$.

In the absence of a trapping potential, and for $l = 0$ and $E = 0$, the solution Eq. (7) becomes valid at all distances. By comparing the long-range behavior of Eq. (7), $\lim_{r\to\infty}\psi_0(r)/r \sim (1 + R^*/r\cot\varphi)$, with the well-known asymptotic form of the

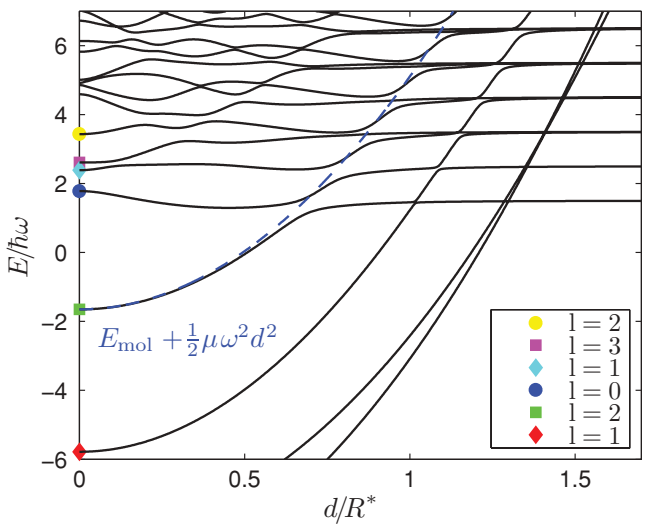

FIG. 3. (Color online) An example correlation diagram calculated for $R^* = 3.68 l_0$ and the short-range phase $\varphi = 0.74\pi$, showing the energy spectrum versus the trap separation. The partial wave number l is given for the lowest states at $d = 0$. As explained in the text, molecular-state energies have an approximately parabolic d dependence, indicated by the dashed line.

s-wave radial wave function, $\lim_{r\to\infty} \psi_0(r)/r \sim 1 - a/r$, we can relate the short-range phase to the scattering length

$$a = -R^* \cot\varphi, \tag{8}$$

which is a measurable physical quantity. We note that R^* determines the typical length scale for the scattering length. In this section, we have focused only on single-channel collisions and without considering internal states of the particles. The present approach is generalized in Sec. III to the realistic multichannel situation.

C. Correlation diagram and trap-induced resonances

To obtain an intuitive understanding of atom-ion collisions, we describe them in terms of correlation diagrams, showing the energy spectrum as a function of the trap separation d (see Fig. 3). Such correlation diagrams in this case connect the asymptotic vibrational states for large trap separation to the molecular and vibrational states at zero trap separation. At large distances we find harmonic-oscillator-like equidistant eigenenergies that are independent of d. Molecular bound states, that correspond to the eigenstates with energies well below the zero-point vibration energy $E_0 = 3/2\hbar\omega$, experience a quadratic shift with distance d. This effect can be easily understood by noting that the bound states $\Psi_{\rm mol}(r)$ are well localized around $r = 0$, and $\langle\Psi_{\rm mol}|H_{\rm rel}^{(d)}|\Psi_{\rm mol}\rangle \approx E_{\rm mol} + \frac{1}{2}\mu\omega^2 d^2$, where $E_{\rm mol}$ is the molecular binding energy at $d = 0$. Besides the given arguments, the quadratic shift in the molecular energy becomes immediately clear in Fig. 4. The molecular potential "hangs" from the relative trapping potential in the low-distance region; thus, increasing (decreasing) d shifts the molecular energy up (down) as d^2.

At some particular distances, the energies of the molecular states become equal to the energies of the vibrational levels (see Fig. 4), and the spectrum exhibits avoided crossings,

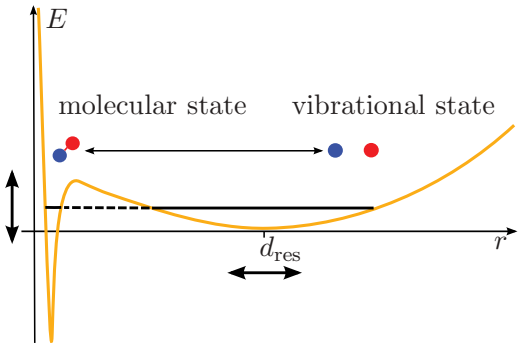

FIG. 4. (Color online) Trap-induced shape resonance: At a certain trap separation $d = d_{\rm res}$, the energy of a molecular bound state degenerates to a trap vibrational energy. The adiabatic eigenenergies exhibit an avoided crossing at this position. The arrows indicate that the molecular energy is shifted if the relative trap position is changed.

known as the trap-induced shape resonances [18]. By slowly changing the trap separation d, we can pass through the resonance adiabatically, converting the trap vibrational states into molecular states and, thus, producing molecular ions. Since this process is reversible, we can coherently control the dynamics of our system by appropriately adjusting the trap distance.

III. QUANTUM-DEFECT THEORY FOR TRAPPED PARTICLES

A. Multichannel formalism

In general, the interaction properties depend on the internal state of two colliding particles. For these internal states we choose a convenient basis in which the two-particle Hamiltonian is diagonal at large particle distance, where the interaction potential is negligible. We then refer to the two-particle basis states as scattering channels. The wave function is decomposed into the chosen basis, which allows us to write Schrödinger's equation in matrix form. In the following we introduce an MQDT formalism, following closely the formulation by F. Mies [19] and adapting it to a situation that includes an external trapping potential. If the same trapping frequencies for atom and ion are assumed, the c.m. and relative degrees of freedom are decoupled. In this case we can describe the relative motion with the close-coupled Schrödinger equation

$$-\frac{\hbar^2}{2\mu}\Delta\mathbf{\Psi}(r) + [\mathbf{W}(r) + \mathbf{U}(\mathbf{r}) - E\mathbf{I}]\,\mathbf{\Psi}(r) = 0, \tag{9}$$

where $\mathbf{I}$ denotes the identity matrix, $\mathbf{W}(r)$ is the interaction matrix

$$W_{ij}(r) \xrightarrow{r\to\infty} \left[E_i^\infty - \frac{C_4}{r^4}\right]\delta_{ij}, \tag{10}$$

which is asymptotically diagonal, with $\{i, j\}$ indicating the channels. The trapping potential $\mathbf{U}(r)$ is diagonal at all distances:

$$U_{ij}(\mathbf{r}) = \tfrac{1}{2}\mu\omega^2(\mathbf{r} - \mathbf{d})^2\delta_{ij}. \tag{11}$$

The matrix $\mathbf{\Psi}(r)$ contains N linearly independent solutions, where N is the number of channels. The threshold energies for the molecular dissociation in channel i are denoted by E_i^∞.

1. Special case: $d = 0$

For $\mathbf{d} = 0$ the external potential is spherically symmetric and the dynamics for different relative angular momenta l is decoupled. We can decompose $\mathbf{F}(r)$ into a partial wave expansion

$$\mathbf{\Psi}(\mathbf{r}) = \sum_l c_l \mathbf{F}_l(r) Y_{l0}(\hat{\mathbf{r}})/r, \tag{12}$$

where for simplicity we consider only the $m = 0$ subspace. The radial wave functions $\mathbf{F}_l(r)$ fulfill

$$[H_l \mathbf{I} + \mathbf{W}(r)]\,\mathbf{F}_l(r) = E\mathbf{F}_l(r), \tag{13}$$

with

$$H_l = -\frac{\hbar^2}{2\mu}\frac{\partial^2}{\partial r^2} + \frac{\hbar^2 l(l+1)}{2\mu r^2} + \frac{1}{2}\mu\omega^2 r^2. \tag{14}$$

In our calculations we model the short-range potential by choosing appropriate short-range phases φ_i for each of the channels. This approach is equivalent to setting $W_{ij}(r) = (E_i^\infty - C_4/r^4)\delta_{ij}$ at all distances. In this case the reference potentials that are necessary to define the MQDT functions [19] can simply be taken as diagonal elements of $\mathbf{W}(r)$: $V_i(l,r) \equiv W_{ii}(r) + \frac{\hbar^2 l(l+1)}{2\mu r^2}$. Given the reference potentials, $V_i(l,r)$, one can associate them with a pair of linearly independent solutions $\hat{f}_i(l,r)$ and $\hat{g}_i(l,r)$ of the single-channel Schrödinger equation that have WKB-like normalization at small distances:

$$\left.\begin{aligned} \hat{f}_i(l,r) &\cong k_i(l,r)^{-1/2}\sin\beta_i(l,r) \\ \hat{g}_i(l,r) &\cong k_i(l,r)^{-1/2}\cos\beta_i(l,r) \end{aligned}\right\} r \sim r_{\min}, \tag{15}$$

where $k_i(l,r) = \sqrt{2\mu[E - V_i(l,r)]}/\hbar$ is the local wave vector and $\beta_i(l,r) = \int^r \mathrm{d}x k_i(l,x)$ is the WKB phase. Here $r_{\min}$ denotes a typical distance where the minima of the realistic potential occur, and the semiclassical approximation is applicable. In our modeling, $r_{\min} \to 0$, and Eq. (15) describes the asymptotic behavior $r \to 0$.

The solution to Eq. (13) can be expressed in terms of a pair of functions, $\hat{\mathbf{f}}_l(r) \equiv \{\delta_{ij}\hat{f}_i(l,r)\}$ and $\hat{\mathbf{g}}_l(r) \equiv \{\delta_{ij}\hat{g}_i(l,r)\}$:

$$\mathbf{F}_l(r) = [\hat{\mathbf{f}}_l(r) + \hat{\mathbf{g}}_l(r)\mathbf{Y}_l(E)]\hat{\mathbf{A}}, \tag{16}$$

where $\mathbf{Y}_l(E)$ is the quantum-defect matrix that represents the effects of the short-range potential, in particular couplings between channels, and is discussed later. The matrix $\hat{\mathbf{A}}$ has constant coefficients and is determined by the boundary conditions at $r \to \infty$. We note that in MQDT the functions $\hat{\mathbf{f}}_l(r)$ and $\hat{\mathbf{g}}_l(r)$ generally describe only the asymptotic ($r \to \infty$) behavior of $\mathbf{F}_l(r)$. Because of our choice of $\mathbf{W}(\mathbf{r})$ and $V_i(l,r)$, however, in our case these functions are valid at all distances.

In analogy to MQDT in free space, we introduce another type of solution, normalized at $r \to \infty$. At large distances, the harmonic potential dominates and the solution vanishing at $r \to \infty$ reads

$$\phi_i(l,r) \overset{r\to\infty}{\longrightarrow} D_\nu(\sqrt{2}r/\xi), \tag{17}$$

where $D_\nu(z)$ is the parabolic cylinder function, $E = E_i^\infty + \hbar\omega(\nu + \frac{1}{2})$, and ξ is the harmonic oscillator length $\xi = \sqrt{\hbar/\mu\omega}$. The two types of solutions, Eqs. (15) and (17), can be related by the MQDT functions $\nu_i(l,E)$ and $\mathcal{N}_i(l,E)$:

$$\begin{aligned}\phi_i(l,r) = \mathcal{N}_i(l,E)[&\cos\nu_i(l,E)\hat{f}_i(l,r) \\ &- \sin\nu_i(l,E)\hat{g}_i(l,r)].\end{aligned} \tag{18}$$

The function $\nu_i(l,E)$ mixes the two solutions of Eq. (15), leading to the exponentially decaying function $\phi_i(l,r)$, whereas $\mathcal{N}_i(l,E)$ provides the overall normalization. In fact the normalization can be calculated directly from $\nu_i(l,E)$ [19]:

$$\mathcal{N}_i(l,E) = \left(\frac{\hbar^2}{2\mu}\frac{\partial\nu_i(l,E)}{\partial E}\right)^{-1/2}. \tag{19}$$

Now the wave function $\mathbf{F}_l(r)$ can be equivalently expressed in terms of solutions $\mathbf{\Phi}_l(r) \equiv \{\delta_{ij}\phi_i^l(r)\}$ normalized at infinity:

$$\mathbf{F}_l(r) = \mathbf{\Phi}_l(r)\mathbf{A}. \tag{20}$$

By comparing Eq. (16) with Eq. (20), one arrives at the following equation:

$$[\mathbf{Y}_l(E) + \tan\boldsymbol{\nu}_l(E)]\,\boldsymbol{N}_l(E)\cos\boldsymbol{\nu}_l(E)\mathbf{A} = 0, \tag{21}$$

where $\boldsymbol{\nu}_l(E) \equiv \{\delta_{ij}\nu_i^l(E)\}$ and $\boldsymbol{N}_l(E) \equiv \{\delta_{ij}\mathcal{N}_i^l(E)\}$. This equation has a nontrivial solution ($\mathbf{A} \neq 0$) if

$$|\mathbf{Y}_l(E) + \tan\boldsymbol{\nu}_l(E)| = 0, \tag{22}$$

which is a standard condition that determines bound states in the MQDT approach. From Eq. (22) one can evaluate eigenenergies in the multichannel case, whereas the eigenstates are given by Eq. (20), with $\mathbf{A}$ determined from Eq. (21). This procedure yields a set of eigenfunctions $\mathbf{F}_{ln}(r) = \mathbf{\Phi}_l(r)\mathbf{b}_{ln}$ and corresponding eigenenergies E_{ln}, where $\mathbf{b}_{ln}$ is a constant vector, and the label n enumerates the solutions:

$$[H_l\mathbf{I} + \mathbf{W}(r)]\mathbf{F}_{ln}(r) = E_{ln}\mathbf{F}_{ln}(r). \tag{23}$$

Similarly to ordinary scalar wave functions, the multichannel eigenstates corresponding to different nondegenerate eigenenergies are orthonormal:

$$\int_0^\infty \mathrm{d}r\mathbf{F}_{ln}(r)^\dagger\mathbf{F}_{lm}(r) = \delta_{nm}. \tag{24}$$

2. Generalization to $d \neq 0$

At nonzero trap separation, the Hamiltonian is no longer rotationally invariant, and the procedure presented in the previous section based on decoupling of states with different values of l does not apply. Nevertheless, we can use the previous solutions at $\mathbf{d} = 0$ to diagonalize the full problem of Eq. (9) at $\mathbf{d} \neq 0$. To this end, the total wave function is decomposed in terms of arbitrary expansion coefficients c_{ln}:

$$\mathbf{F}(\mathbf{r}) = \sum_{ln} c_{ln}\mathbf{F}_{ln}(r)Y_{l0}(\hat{\mathbf{r}})/r. \tag{25}$$

Substituting this into Eq. (9) and setting $\mathbf{d} = d\mathbf{e}_z$ gives the set of coupled equations

$$\left(E_{ln} + \frac{1}{2}\mu\omega^2 d^2\right)c_{ln} + \mu\omega^2 d\sum_{l'n'} D_{ln}^{l'n'}c_{l'n'} = Ec_{ln}, \tag{26}$$

which in principle can be solved numerically with standard methods for matrix diagonalization. Here

$$D_{nl}^{l'n'} \equiv \langle Y_{l0}|\cos\theta|Y_{l'0}\rangle \int_0^\infty \mathrm{d}r \mathbf{F}_{ln}(r)^\dagger r \mathbf{F}_{ln'}(r) \tag{27}$$

and

$$\begin{aligned}\langle Y_{l0}|\cos\theta|Y_{l'0}\rangle &= \int \mathrm{d}\Omega Y_{l0}^*(\hat{\mathbf{r}})\cos\theta Y_{l'0}(\hat{\mathbf{r}}) \\ &= \frac{l+1}{\sqrt{(2l+1)(2l+3)}}\delta_{l+1,l'} \\ &\quad + \frac{l}{\sqrt{(2l-1)(2l+1)}}\delta_{l-1,l'}.\end{aligned} \tag{28}$$

3. *Parametrization of* $\mathbf{Y}_l(E)$ *and the frame transformation*

In the regime of ultracold collisions, the variation of the total energy E and the height of the angular momentum barrier (for the lowest partial waves, which are important in the ultracold regime [9]) are much smaller than the depth of the potential at $r \sim r_{\min}$, where the matrix $\mathbf{Y}_l(E)$ is defined. Therefore, it is justified to neglect the dependence of $\mathbf{Y}_l(E)$ on both energy and angular momentum and to set $\mathbf{Y}_l(E) \cong \mathbf{Y}$. In this way, by determining the matrix $\mathbf{Y}$ at a single value of energy, we may describe the atom-ion collisions in the whole regime of ultracold temperatures.

This paper considers collisions of an alkali metal atom with an alkaline-earth metal ion in their electronic ground states. Hence, the asymptotic channel states that are used in the Schrödinger equation, Eq. (13), can be characterized by the hyperfine quantum numbers f_1,m_{f_1} and f_2,m_{f_2} for ion and atom, respectively, and by the angular-momentum quantum numbers l and m_l of the relative motion of the atom and ion c.m. In the rest of this section, those channels are labeled as $\alpha = \{f_1 f_2 m_{f_1} m_{f_2} l m_l\}$.

At short distances, the potential matrix becomes diagonal in the molecular basis characterized by the total electron and nuclear spins and their projections, because the short-range forces depend on the electronic configuration of the entire atom-ion molecular complex. In fact, the molecular potentials that correlate with atom and ion electronic ground states at large distances depend only on the total electron spin S [9]. For our choice of species, the electronic configurations are identical, as in the collision of two hydrogen atoms. Thus, S can take the values 0 (singlet configuration) and 1 (triplet configuration). Hence, the quantum-defect matrix $\mathbf{Y}$, which contains the full interaction information, can be parametrized with only two constants, the singlet and triplet scattering lengths, a_s and a_t, respectively. These constants depend only on the species.

The approach is to apply a frame transformation to find $\mathbf{Y}$ in the basis of hyperfine states [20,21]. As shown in Ref. [9], this approximation is very accurate for atom-ion collisions due to a clear separation of length scales associated with the short- and long-range forces. On the one hand, exchange interaction becomes significant only at distances of the order of a few tens of a_0 (atomic units), when the electronic wave functions of atom and ion begin to overlap. On the other hand, the polarization forces are very long-ranged and they are modified by the presence of the centrifugal barrier only at large distances of the order of R^*.

B. Reduction to an effective single-channel model in the case of $a_s \approx a_t$

The off-diagonal matrix elements in the quantum-defect matrix $\mathbf{Y}$ are proportional to the "coupling" scattering length, which is defined as $1/a_c = 1/a_s - 1/a_t$ [9]. Therefore, in the case of $a_s \approx a_t$, the coupling between channels is weak and the multichannel description can be effectively reduced to a single-channel model. To this end, we solve the multichannel problem at $d = 0$ and find the corresponding eigenenergies E_{nl} and eigenstates $\mathbf{F}_{nl}(r)$ from Eqs. (21) and (22). If the mixing between channels is weak, in each of the eigenfunctions $\mathbf{F}_{nl}(r)$, there is only one channel that dominates; that is, the vector $\mathbf{b}_{ln}$ has only one element that is close to unity. We divide the total multichannel spectrum into N distinct subsets according to the channel that gives the leading contribution to $\mathbf{F}_{nl}(r)$, and for each of the subsets we determine the effective short-range phase φ_l^{eff} (or the scattering length, $a_l^{\mathrm{eff}} = -R^* \cot\varphi_l^{\mathrm{eff}}$). This is done by matching the multichannel spectrum E_{nl} in each of the subsets with the single-channel spectrum generated by Eq. (5) with the quantum-defect parameter φ_l^{eff}. In the limit of zero coupling between channels, the effective scattering length a_l^{eff} is equal to $a_s = a_t$. In the presence of weak coupling, a_l^{eff} is generally different from a_s and a_t, since the asymptotic channels typically correlate both to singlet and triplet molecular states at small distances. This procedure yields a set of N short-range phases $\{\varphi_l^{\mathrm{eff}}\}$, which are used at a later stage in the single-channel calculations. We note that the effective phases $\{\varphi_l^{\mathrm{eff}}\}$ depend on the relative angular momentum, and in principle they weakly depend on the energy. We have verified, however, that within the considered range of energies limited to the bound states close to the dissociation threshold, and to a few tens of the lowest vibrational states, the variations of $\varphi_l^{\mathrm{eff}}(E)$ with the energy are negligible.

For collisions occurring when only a single open channel exists, the remaining closed channels are typically only weakly coupled to the open channel (apart from the case of resonances), and the resulting multichannel wave function is dominated by the open-channel component. The situation changes, however, when there are more open channels, and channel mixing can be significant. This issue was investigated numerically by picking the specific ion and atom pair $^{135}\mathrm{Ba}^+$-$^{87}\mathrm{Rb}$ and the trapping frequency $\omega_i = \omega_a = 2\pi \times 30$ kHz. We have considered collisions within the $m_F = 3$ subspace, assuming that initially the particles are prepared in the channel $\alpha_1 = \{f_i = 1, m_{f_i} = 1, f_a = 2, m_{f_a} = 2\}$. This choice is relevant for our modeling of the quantum gate, as shown later. For the collision energies above the dissociation threshold of channel α_1, a second open channel exists, with $\alpha_2 = \{f_i = 2, m_{f_i} = 2, f_a = 1, m_{f_a} = 1\}$. In this case, the admixture of the two remaining closed channels is negligible, whereas the contribution of both channels α_1 and α_2 in the multichannel eigenstates is typically large, and the contributions from α_1 and α_2 cannot be separated. The only exception is the case of similar a_s and a_t, in which the interchannel coupling $1/a_c$ is small, and the multichannel eigenstates are dominated by the single-channel contributions.

We estimate the validity of the single-channel approximation by calculating the overlap of the exact multichannel and single-channel wave functions, in the range of trap separations

d, that are interesting for our dynamics. The minimum over d yields some overall fidelity related to the reduction to the single-channel model. For similar singlet and triplet phases, we have $\phi_l^{\text{eff}} \approx \phi_s \approx \phi_t$, and the multichannel wave functions differ from their single-channel counterparts by the presence of negligible contributions in the channels other than the dominating one. The relative contributions of individual channels are given by the vectors $\mathbf{b}_{ln}$ that are obtained in the calculation of eigenstates at $d = 0$. When $d > 0$, one has to take into account that the multichannel wave functions are linear combinations of the solutions at $d = 0$ [see Eq. (25)], and the overlap between single- and multichannel eigenstates is a linear combination of the overlaps calculated at $d = 0$ with the expansion coefficients given by $|c_{ln}|^2$.

Resonances occurring at $d = 0$ can lead to significant channel mixing for few states, although the average fidelity is very high. The more these highly mixed states contribute to the wave functions, the larger is the error of the model. For the error estimation used in this work, only the trap ground state at maximal d and a molecular state at minimal d of interest are used. The two fidelities are found to lie in the same range; thus, we take the minimum of them and assume the result as a lower bound for the fidelity at intermediate distances. We have additionally verified that reductions to the single-channel model work best for positive values of singlet and triplet scattering lengths around R^*.

IV. ATOM-ION DYNAMICS

Traps for individual ultracold atomic particles used in schemes for quantum information processing provide, in most cases, for the ability to manipulate the particles' motion via appropriate tuning of external trap parameters. This case is particularly true for optical lattices and Paul traps, where field polarizations and intensities can be changed to control the shape and position of the traps to a high degree of accuracy. Our proposal relies on these standard techniques, thereby introducing the innovative aspect of combining traps for ions and atoms. As already discussed elsewhere [12], the physical mechanisms generating the traps for ions and atoms are different and they lead, under appropriate conditions, to independent microscopic traps, which can be modeled as follows.

In this section, the dynamics is described by introducing a time-dependent trap displacement $d(t)$. Below a certain distance $d \sim R^*$, the eigenenergies of the system start to depend on the spin state as well as on d itself, and positions of trap-induced resonances are determined by the internal state of both particles. In this way, trap displacement can be used for spin-dependent control of the atom-ion system.

A. Landau-Zener theory

The Landau-Zener formula gives a basic understanding of the atom-ion dynamics in the vicinity of trap-induced shape resonances. It describes a general two-level system whose eigenstates $|\Psi_1\rangle$ and $|\Psi_2\rangle$ are coupled by some kind of interaction, and in which the two eigenlevels E_1 and E_2 form an avoided crossing when varying an external parameter. In the current work, this external parameter is the trap displacement d. The probability of a nonadiabatic passage of the crossing [12],

$$P_{\text{na}} = \exp\left(-2\pi \frac{|\langle\Psi_1|H|\Psi_2\rangle|^2}{\hbar|\dot{d}\,\partial E_{12}/\partial d|}\right), \tag{29}$$

depends on the coupling matrix element, the velocity $\dot{d}$ of passage of the resonance, and the relative slope $\partial E_{12}/\partial d$ of the levels, where $E_{12} = E_1 - E_2$. A fast passage of the avoided crossing ($P_{\text{na}} \approx 1$) results in a nonadiabatic evolution, preserving the shape of the wave function. At small velocities the resonance is passed adiabatically ($P_{\text{na}} \approx 0$); that is, the system follows its eigenenergy curves. In the trapped atom-ion system, for certain trap separations, the energy of some molecular bound states becomes equal to harmonic-oscillator energies, resulting in the avoided crossings. If such an avoided crossing is passed adiabatically, then the initial harmonic-oscillator state with atom and ion located in their separated traps can evolve into a molecular bound state, where the atom and ion are trapped in a combination of the two external potentials. This process is reversible and is used in Sec. V to realize an entangling two-qubit operation.

To precisely predict the outcome of a collision process, in our simulations we have calculated the time evolution numerically using the Landau-Zener formula only as a guide to estimate the relevance of the avoided crossings for the transfer process. Since the energy of the molecular bound states changes according to $E_{\text{mol}}(d) \approx E_{\text{mol}}(0) + 1/2\mu\omega^2 d^2$ (see Fig. 3), deeply bound states can cross vibrational states only at large d. In this case avoided crossings are very weak because ΔE decays exponentially with the trap distance [12]. Hence, the deeply bound states have no relevance for the dynamics and in the current simulations only shallow bound states that are closest to the dissociation threshold have been included.

B. Full dynamics in the single-channel model

In the case of similar a_s and a_t, when the effective single-channel description is applicable, the dynamics of the controlled atom-ion collision can be desrcibed by the following time-dependent Hamiltonian:

$$H_{\text{rel}}^{(d)}(t) = H_{\text{rel}}^{(0)} + \tfrac{1}{2}\mu\omega^2 d(t)^2 - \mu\omega^2 d(t) z. \tag{30}$$

We decompose the corresponding time-dependent wave function in the basis of the eigenstates at $d = 0$

$$|\Psi(t)\rangle = \sum_{nl} c_{nl}(t)\big|\Psi_{nl}^{(0)}\big\rangle, \tag{31}$$

in analogy to Eq. (25). Substituting into the Schrödinger equation, we obtain a set of coupled differential equation for the expansion coefficients c_{nl}:

$$\begin{aligned} i\hbar\dot{c}_{n'l'} &= \sum_{nl} c_{nl}(t)\Big\{\Big[E_{n'l'}^{(0)} + \tfrac{1}{2}\mu\omega^2 d(t)^2\Big] \\ &\quad \times \delta_{n,n'}\delta_{l,l'} - \mu\omega^2 d(t) D_{nl}^{n'l'}\Big\}, \end{aligned} \tag{32}$$

where $D_{nl}^{n'l'} = \langle\Psi_{n'l'}^{(0)}|z|\Psi_{nl}^{(0)}\rangle$ is the dipole matrix element, which in the context of the multichannel formalism is defined

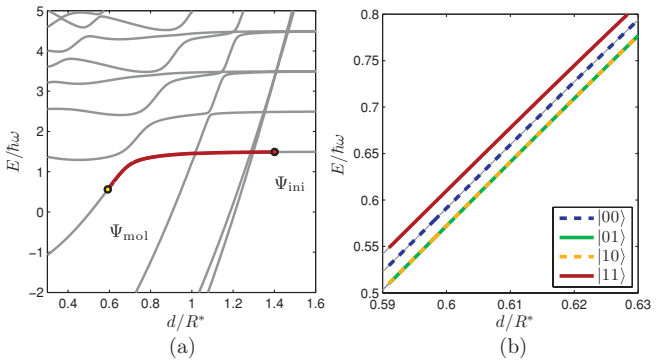

FIG. 5. (Color online) Correlation diagrams for $a_s = 0.90$ and $a_t = 0.95$, where for each of the qubit pairs we subtract the threshold energy of the corresponding channel. The energy curve followed in the adiabatic process is marked with a thick line between $\Psi_{\rm ini}$ and $\Psi_{\rm mol}$ in part (a). We only show the complete diagram for the $|11\rangle$ channel. Small energy differences of the channels around $d = d_{\rm min}$ can be seen in the close-up (b). These differences are the basis of our proposal for realizing an atom-ion phase gate.

in Eq. (27). We determine the radial part of the single-channel wave functions and the eigenenergies $E_{nl}^{(0)}$ with the Numerov method [22], using the effective short-range phase as a boundary condition at minimal distance. From the wave functions, one can calculate the matrix elements $D_{nl}^{n'l'}$. Inserting these elements into Eq. (32), we are able to solve the equation for the coefficients numerically using standard calculations. Thereby we verify in each case that our basis, limited by the maximal values of quantum numbers l and n, is large enough and that the results do not change when increasing the basis.

By comparing exact numerical dynamics with the results predicted by the Landau-Zener theory, an error of about 0.5% was found, for example, for the probability of a fast, diabatic passage of the avoided crossing at $d = 1$ in the spectrum of Fig. 5(a), with a speed of 1 mm/s. Similar good agreement was observed in the adiabatic limit, and discrepancies of the order of 10% were found only for intermediate speeds. These discrepancies might be due to the complexity of the spectrum, which makes it impossible to isolate an avoided crossing between two eigenstates from the influence of the rest of the eigenstates. Thus, the Landau-Zener theory is not applicable for quantum gate calculations performed, for example, in Sec. V E1. Also, faster processes lead to excitations to higher vibrational states that cannot be described by the Landau-Zener theory.

V. QUANTUM GATE

A. Qubit states

In this section the model of the spin-state-dependent atom-ion collisions are applied to construct a two-qubit controlled-phase gate. Qubit states are encoded in hyperfine states of atom and ion. According to previous notation, a given two-particle spin state is referred to as a channel $\alpha = \{f_i f_a m_{f_i} m_{f_a} l m_l\}$. The total spin projection $m_f = m_{f_i} + m_{f_a}$ is a conserved quantity during the collision. Therefore, two states of unlike m_f cannot be coupled. In our case it is convenient to pick the

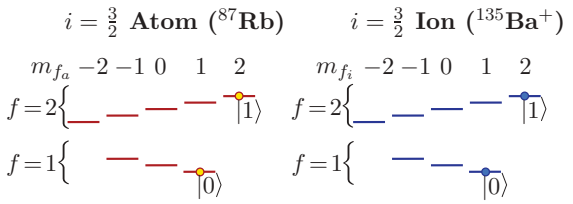

FIG. 6. (Color online) Specific choice of the qubit states out of the manifold of hyperfine spin states of a ^{87}Rb atom and a ^{135}Ba$^+$ ion.

computational basis states

$$\begin{aligned} |0\rangle_{i,a} &= |f_{i,a}=1, m_{f_{i,a}}=1\rangle_{i,a} \\ |1\rangle_{i,a} &= |f_{i,a}=2, m_{f_{i,a}}=2\rangle_{i,a} \end{aligned} \tag{33}$$

according to Fig. 6, leading to the two-qubit states

$$\begin{aligned} |00\rangle &= |f_i=1, m_{f_i}=1, f_a=1, m_{f_a}=1\rangle = |1,1,1,1\rangle, \\ |01\rangle &= |f_i=1, m_{f_i}=1, f_a=2, m_{f_a}=2\rangle = |1,1,2,2\rangle, \\ |10\rangle &= |f_i=2, m_{f_i}=2, f_a=1, m_{f_a}=1\rangle = |2,2,1,1\rangle, \\ |11\rangle &= |f_i=2, m_{f_i}=2, f_a=2, m_{f_a}=2\rangle = |2,2,2,2\rangle. \end{aligned} \tag{34}$$

Each of the two-qubit states is represented by a scattering channel. The state $|00\rangle$ has $m_f = 2$ and is coupled to seven other channels, which have higher dissociation energies and therefore remain closed for $|00\rangle$ collisions. Thus, the state $|00\rangle$ is stable with respect to spin-changing collisions. The channels $|01\rangle$ and $|10\rangle$, belonging to the $m_f = 3$ subspace, are coupled to each other and to two other channels that are closed for both $|01\rangle$ and $|10\rangle$ collisions. There is no coupling for the state $|11\rangle$, since it is the only state in the $m_f = 4$ subspace. In this way our choice of the qubit states minimizes the possibility of spin-changing collisions, and the only process that can lead to potential losses is the inelastic collision $|10\rangle \rightarrow |01\rangle$.

B. Dynamics of four isolated channels

Our multichannel theory describes collisions between atom and ion for general spin states of particles, in particular for the four qubit states introduced in Eq. (34). For simplicity of the numerical calculations, we do not perform the full multichannel dynamics here but rather we focus on the regime of applicability of the effective single-channel model, described in Sec. III B. For every choice of parameters assumed in our calculations, we verify that the coupling to other spin states can be neglected. The total Hamiltonian including external degrees of freedom, for the subspace corresponding to our computational basis, reads

$$\begin{aligned} H = {} & H_{00} \otimes |00\rangle\langle 00| + H_{01} \otimes |01\rangle\langle 01| \\ & + H_{10} \otimes |10\rangle\langle 10| + H_{11} \otimes |11\rangle\langle 11|. \end{aligned} \tag{35}$$

We denote a qubit channel by $|A\rangle$ with $A \in \{00, 01, 10, 11\}$. Linear combinations of the computational basis states form a general two-particle state $|\Psi\rangle = \sum_A a_A |\Psi^A\rangle |A\rangle$, where $|\Psi^A\rangle$ denotes the quantum state of the atom-ion relative motion for the channel $|A\rangle$. Obviously, the time evolution of $|\Psi\rangle$,

$$|\Psi(t)\rangle = \sum a_A e^{-iE_A t/\hbar} |\Psi^A(t)\rangle |A\rangle, \tag{36}$$

is determined by the dynamics of the spatial part of the wave function $|\Psi^A(t)\rangle$, which we evaluate from Eq. (32). On the other hand, the phases due to the differences in threshold energies E_A in each of the channels do not lead to state-dependent dynamics and can be eliminated by single-qubit operations (see discussion in the next subsection).

C. Phase gate process

The two-qubit phase gate is represented by the transformation

$$\begin{aligned} |00\rangle &\xrightarrow{\text{Interaction}} e^{i\phi_{00}}|00\rangle \xrightarrow{U_S} |00\rangle, \\ |01\rangle &\longrightarrow e^{i\phi_{01}}|01\rangle \longrightarrow |01\rangle, \\ |10\rangle &\longrightarrow e^{i\phi_{10}}|10\rangle \longrightarrow |10\rangle, \\ |11\rangle &\longrightarrow e^{i\phi_{11}}|11\rangle \longrightarrow e^{i\phi}|11\rangle, \end{aligned} \tag{37}$$

performed on the computational basis states. The first step is the controlled interaction of atom and ion that leads to a specific phase for each two-qubit state. By applying the single-qubit transformation U_S we can undo three of these phases and assign the total gate phase

$$\phi = \phi_{00} + \phi_{11} - \phi_{01} - \phi_{10} \tag{38}$$

to the $|11\rangle$ state [23]. If this phase equals π, the phase gate, combined with single-qubit gates, is a universal gate for quantum computation, because it is equivalent to a CNOT gate. It is possible to realize this phase gate scheme within our single-channel model, since the transformation of each two-qubit basis state can be treated separately.

For our gate scheme, atom and ion are initially prepared in the motional ground state of their respective traps. The channel phases are gained by the control of the relative motion of atom and ion during the collision. Ideally we aim at obtaining back the motional ground state at the end of the gate process, so that the phase accumulated by relative motion is assigned to the qubit state.

D. Gate fidelity

The fidelity definition is based on the overlap of the initial state of relative motion $|\Psi^A_{\text{ini}}\rangle$ with the final state $|\Psi^A(T)\rangle$. In an ideal process, these states are equal up to a state-dependent phase. The fidelity needs to account for this phase. For one channel A and at zero temperature, according to Ref. [24] we can define the fidelity F_A as follows:

$$F_A = \tfrac{1}{2}\left[1 - \left|\left\langle \Psi^A_{\text{ini}} \middle| \Psi^A(T)\right\rangle\right| \cos(\pi - \Delta\phi_A)\right], \tag{39}$$

where $\Delta\phi_A = \phi_A(T) - \phi'_A$ is the difference between the desired channel phase ϕ'_A and the phase $\phi_A(T)$ obtained by actual time evolution. In the following, it is assumed that, according to Eq. (37), the phases for the channels $|00\rangle$, $|01\rangle$, and $|10\rangle$ are undone perfectly due to the single-qubit rotations leading to $\Delta\phi_{00} = \Delta\phi_{10} = \Delta\phi_{01} \equiv 0$, while $\Delta\phi_{11}$ is nonzero. Hence, for channels $|00\rangle$, $|01\rangle$, and $|10\rangle$, the fidelity is restricted only by the overlap between initial and final states, while for state $|11\rangle$ we additionally require that the total gate phase, computed from the single-channel phases with Eq. (38), is $\phi = \pi$.

We can further define the overall gate fidelity as

$$F_{\text{gate}} = \min_A F_A, \tag{40}$$

since in our model the channels are decoupled (spin-changing collisions are neglected).

E. Adiabatic regime

The adiabatic dynamics can be understood with the help of the correlation diagrams introduced in Sec. II C. Our gate scheme aims at an adiabatic transfer from an initial oscillator state Ψ_{ini}, to a molecular state Ψ_{mol}, and back to the initial state. This transfer is achieved by a variation of the trap distance across an appropriate avoided crossing, which we choose after investigating the correlation diagram. For example, the resonance at the trap distance $d \sim 0.7$ in Fig. 5(a) appears strong enough and we use it in numerical calculations in the following. During the transfer process each logical basis state acquires a different phase, since the energies of molecular states depend on the channel [see Fig. 5(b)]. The phase accumulated for each channel in an adiabatic transfer process is given by the integral

$$\phi^A_{\text{pot}} = -\frac{1}{\hbar}\int_{t_{\min}}^{t_{\max}} E^A(t)\mathrm{d}t, \tag{41}$$

where E^A is the energy of the adiabatic eigenstate depicted as a function of d in Fig. 5 (thick curve). In the adiabatic regime, excitations to higher vibrational states are avoided by keeping the velocity $\dot{d}$ small compared to the characteristic velocity of the harmonic motion in the trap: $\dot{d} \ll \sqrt{\hbar\omega/\mu}$. On the other hand, the velocity across weaker resonances at larger distances is chosen high enough to pass them diabatically, as seen in Fig. 5. We want to find a particular function $d(t)$, which, if applied to the trapped atom-ion system, results in a desired total gate phase while ensuring diabatic passage of the weak resonances as well as adiabatic passage of the strong resonance. Since the total phase depends on the difference between single-channel phases [see Eq. (38)], the gate speed in fact is determined by the differences in the potential energy curves of unlike channels.

For the sake of concreteness we assume specific values of the singlet and triplet scattering lengths in such a way that the single-channel effective model is applicable. For our calculations we chose $a_s = 0.90R^*$ and $a_t = 0.95R^*$. According to the procedure described in Sec. III B, the estimate of the error introduced by the model is 2×10^{-3}. For singlet and triplet scattering lengths that differ by more than 10%, the channel mixing is already significant and does not allow for a single-channel description.

Actually, the singlet and triplet scattering lengths are uniquely determined by the specific choice of the atom-ion system we describe. Thus far these parameters have not been measured experimentally for any atom-ion system. However, as soon as the accurate values of a_s and a_t are determined, one can repeat the calculations with the physically correct parameters, which may require going beyond the single-channel model and including the full multichannel dynamics according to Sec. III.

Assuming the single-channel effective model, we first compute a correlation diagram for each of the channels, which

is done by diagonalizing the Hamiltonian in the basis of eigenstates evaluated at $d = 0$. The result is depicted in Fig. 5(a) for the $|11\rangle$ channel. The diagrams show small differences in the molecular states at small distances [Fig. 5(b)], since the energy of the molecular states depends on the atom-ion spin configuration (the qubits).

1. Numerical simulation of an adiabatic phase gate

In our simulation of the gate process the initial and final trap separations coincide: $d(0) = d(T) = d_{\max}$. We assume that initially each of the atom and the ion are in the ground state of its own trap. The distance $d_{\max}$ is determined in such a way that there are no bound states in the vicinity of $d_{\max}$ that would influence the harmonic-oscillator ground state.

The controlled time evolution of our atom-ion system requires the appropriate adjustment of the distance $d(t)$ between the two trapping potentials as a function of time. The slope of this function is essential for the result.

In order to follow the energy curve depicted in Fig. 5(a), we construct a specific function $d(t)$. We start at $d_{\max}$ with an initial velocity $d'_1 = 0.5R^*/(\hbar/E^*)$, which is large enough to traverse weaker resonances diabatically. However, much larger velocities would cause unwanted motional excitations in the trap. At $d = 0.95R^*$, the velocity is decreased to $d'_2 = 0.1R^*/(\hbar/E^*)$ in order to adiabatically convert the trap state into a molecular bound state using a stronger resonance. The curve is followed down to some minimal distance $d_{\min}$. Then the reversed pulse brings the system to the initial trap separation. Figure 7(a) shows the complete $d(t)$ function. It is known that sharp kinks can cause motional excitations; therefore, we use a smooth function $d(t) = \tilde{d} + 1/2(d'_1 + d'_2)t \pm \sqrt{(d'_1 - d'_2)^2 t^2 + C^2}$ to change between two slopes $d'_{1,2} = 0.5$ and $0.1R^*/(\hbar/E^*)$. Here, the $+$ $(-)$ sign is used for increasing (decreasing) slope, $\tilde{d}$ is an offset, and C is a parameter adjusting the curvature at the kink around the turning point at $d_{\min}$ $d(t) \sim t^2$.

We can now compute the solution of the Schrödinger equation numerically at a given time by solving Eq. (32) with

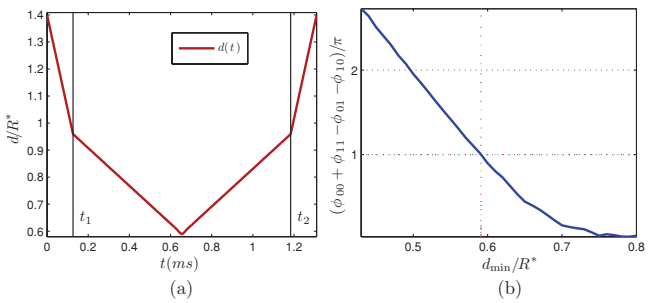

FIG. 7. (Color online) (a) The function $d(t)$ starts at $d_{\max} = 1.4R^*$ with a slope of $d'_1 = 0.5R^*/(\hbar/E^*)$ large enough to diabatically pass weaker resonances. The velocity is changed to around $d = 0.95R^*$ to $d'_2 = 0.1R^*/(\hbar/E^*)$ to ensure an adiabatic traversal of a stronger resonance. The system is brought to the initial distance with the reversed pulse and the kinks are smoothed to avoid motional excitations. The characteristic unit of speed is $R^*/(\hbar/E^*) = 2.05$ mm/s. (b) Gate phase as a function of $d_{\min}$ using the described $d(t)$ shape. We find that with $d_{\min} = 0.591$ a gate phase of $\phi = 1.009\pi$ is reached.

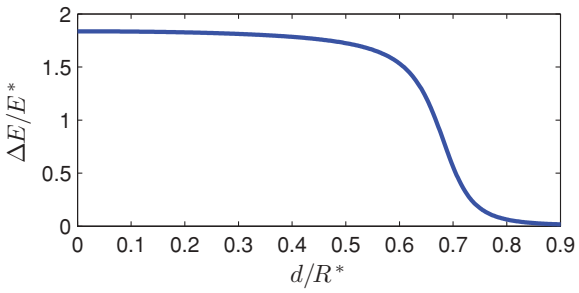

FIG. 8. (Color online) Energy difference as a function of trap separation. For $d \lesssim 0.3R^*$ the function is practically constant, which, for the phase gate process, means that bringing the traps closer than $d_{\min} \sim 0.3R^*$ does not lead to a significant advantage.

standard numerical routines. This yields the gate phase which, for example, can be adjusted by a variation of $d_{\min}$. This phase is in fact a phase difference accumulated due to the energy splitting

$$\Delta E = E^{00}_{\mathrm{mol}} + E^{11}_{\mathrm{mol}} - E^{01}_{\mathrm{mol}} - E^{10}_{\mathrm{mol}}, \tag{42}$$

shown in Fig. 8 as a function of trap separation; the larger ΔE, the faster a phase difference is reached. Thus, decreasing $d_{\min}$ increases the phase, as seen in Fig. 7(b). We find a gate phase of $\phi = 1.009\pi$ at $d_{\min} = 0.591R^*$. The corresponding gate fidelity is $F_{\mathrm{gate}} = 0.994$ according to Eq. (40). The process takes time $T = 9.14\hbar/E^*$, which equals $T = 1.31$ ms for our choice of the trapping frequency, $\omega = 2\pi \times 30$ kHz, and the masses and hyperfine structure of the ^{87}Rb atom and the ^{135}Ba$^+$ ion. We show the population of the instantaneous eigenstates in Fig. 9. At $d_{\max}$ the trap ground state is labeled with $n = 1$. The system is initialized in this state. At half gate time the quantum state changes to $n = 4$, which is the molecular state at $d_{\min}$. Finally, at the end of the gate process, the initial state has been almost perfectly obtained.

F. Fast gate using optimal control

Quantum optimal control techniques are powerful tools in that they allow the fidelity of a time evolution process to be increased by finding an appropriate pulse shape for some external control parameter. The outcome of the controlled collision of an atom and an ion is very sensitive to the particular shape of the time dependence in the trap distance, $d(t)$. It is hard to manually design a specific function $d(t)$ that leads to a phase gate fidelity very close to unity.

The most significant problem in our specific example calculation results from a relatively weak resonance at $d_0 \approx 1R^*$, which we want to pass in a nonadiabatic way. We could not find an optimal constant slope that brings us from the trap state at $d > d_0$ to the trap state with $d < d_0$ across the resonance without losses. Large velocities lead to excitations of energetically higher states, while the consequence of smaller velocities is a non-negligible population of the molecular state that crosses the trap state. This population is not fully recovered on the way back. In Sec. V E1 we nevertheless find a process that yields a gate fidelity of $F_{\mathrm{gate}} = 0.994$.

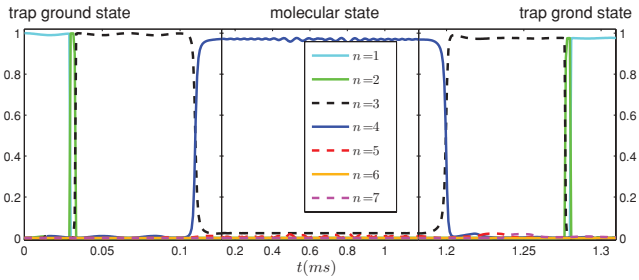

FIG. 9. (Color online) Population of the most important adiabatic eigenstates for the qubit channel $|11\rangle$ during the adiabatic gate process (the remaining channels show similar behavior). States are labeled according to their energy in the correlation diagram in ascending order. The initial state at $t = 0$ is the relative-motion ground state in the trapping potential for $d = d_{\max}$. The label of this state is set to $n = 1$. The molecular state marked in Fig. 5(a) then bears the label $n = 4$. Around a crossing, the labels of molecular and trap states switch because their energies change order. Our goal is to follow the energy curve marked between Ψ_{ini} and Ψ_{mol} in Fig. 5(a). We observe that indeed two resonances are passed diabatically. At $t = T/2$ the state $n = 4$ is reached with relatively high fidelity, which means that a molecular ion is formed here. At $d(T) = d_{\max}$ the initial state is regained (the state-dependent phase of the final state is not depicted here). To better show the features of the curves, the time axis is squeezed between $t_1 = 0.12$ ms and $t_2 = 1.18$ ms, where the velocity is lower (see Fig. 7).

With optimal control, not only can we find a pulse shape that produces a satisfactory gate fidelity, but we can also go beyond the adiabatic regime and reduce the gate time. By applying larger velocities, we allow for excitations to higher energy levels. By making use of interference effects, an appropriate $d(t)$ pulse shape can undo these excitations in the final state of the process.

This optimal pulse shape is found here with an iterative optimization algorithm called intermediate feedback control, which is introduced in Ref. [13]. We start with an initial guess for the control function $d(t)$, which in general does not yield a satisfactory fidelity. The fidelity of the process is increased in every iteration step by updating $d(t)$. We divide the time axis in small time steps dt. At each time step we evolve the wave function forward in time using the Crank-Nicholson scheme [25]. The update of $d(t)$ is successively performed in every time step.

1. *Enhancing the fidelity of the adiabatic gate*

The adiabatic gate process of Sec. V E 1 has the fidelity $F_{\text{gate}} = 0.994$. With only three iterations of the optimal control algorithm, we can enhance this fidelity to $F_{\text{gate}} = 1 - 7 \times 10^{-4}$, which even exceeds the validity of the underlying single-channel model. The gate phase is improved to 1.0026π. The optimized function $d(t)$ shows small-scale variations ("wiggles") that are a typical feature of this particular optimization algorithm. These wiggles have amplitude $\sim 0.002 R^* \approx 0.6$ nm and happen on a time scale of the order of 10 μs. This amplitude is smaller than the uncertainty of the ion-trap center position in up-to-date experimental realizations.

2. *Fast gate scheme*

It is desirable to reduce the gate time to a minimum. In our case this minimum is given by the least time that is required for accumulating the gate phase $\phi = \pi$. We profit from the energy differences of the molecular states for the different channels. The differences are largest at small distance $d_{\min}$, but below $d \approx 0.3 R^*$ they are practically constant. The fastest possible gate must effectively transport the atom-ion relative wave function into a molecular state, where the gate phase is accumulated during a certain time. The gate ends with a reversed pulse and brings the system to the initial trap ground state, while the logical phase is preserved.

The optimal control algorithm can be used to build such a gate process. As a first step, we design $d(t)$, changing the quantum state of atom and ion from the trap ground state at $d_{\max} = 1.4 R^*$ to the molecular state at $d_{\min} = 0.3 R^*$, for all channels during the transport time t_{trans}. The optimization objective $J = \sum_A 2\text{Re}\{\langle \Psi^A(t_{\text{trans}}) | \Psi^A_{\text{mol}} \rangle\}$ for this step aims at maximizing the overlap of the time-evolved state with the desired molecular state. The second step is a stationary evolution at $d_{\min}$, where the main part of the differential phase is accumulated. Subsequently we perform the reverse of the initial pulse. The combined $d(t)$ pulse is shown in Fig. 10(a).

The total gate time is $T = 346$ μs. With respect to the adiabatic case this indicates a reduction by a factor of 4. Since our scheme makes use of the channel energy differences in the molecular state at $d = d_{\min} = 0.3 R^*$, we can estimate a quantum speed limit of $T_{\text{limit}} = \pi\hbar/\Delta E$ for this process, with ΔE from Eq. (42), which gives the minimal gate time and neglects transport durations and infidelities of the molecular state's population. In our example this limit is $T_{\text{limit}} \approx 250$ μs. Our gate process time lies very close to this value, considering an overall transport time of $2t_{\text{trans}} = 158$ μs. We note that a part of the phase is accumulated during the transport phase, since we already enter the regime where the energy differences become significant.

Further reduction of the transport time may be possible, but the optimization algorithm used here stopped converging in reasonable time for larger transport velocities. However, we have already shown that the process could be significantly accelerated by using optimal control techniques.

3. *Perspectives for further improvement*

Certainly the gate speed would improve if the difference between singlet and triplet scattering lengths was larger than assumed in the example calculation. In a general case one can use the current multichannel formalism for an accurate description of the dynamics beyond the single-channel approximation. We point out that the essential parameters a_s and a_t are still unknown and they must be measured experimentally in order to do realistic calculations for specific systems. However, this work demonstrates the feasibility of an ion-atom quantum gate, even one based on the simplified scheme we assume for the purpose of calculations.

Further possibilities occur for very different values of a_s and a_t. In this case the $|10\rangle$ and $|01\rangle$ states in particular are coupled strongly. In this case optimal control mechanisms can be used to suppress effects of spin-changing collisions in the final state in order to realize a phase gate. The coupling of $|01\rangle$

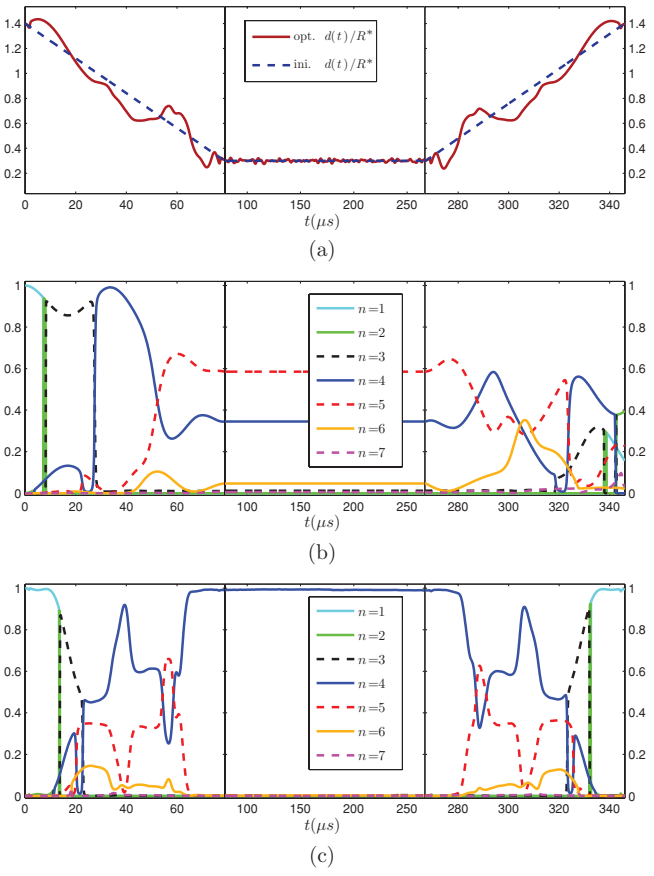

FIG. 10. (Color online) (a) Optimized $d(t)$ function and initial guess (dashed) for the fast gate process. The initial state is the trap ground state at $d_{\max}$. The populations of the adiabatic eigenstates are changed by the optimization process. (b) After the initial guess pulse is applied, higher vibrational and also molecular states become populated. (c) These excitations are prevented or undone using the optimized pulse. In this case, at $d_{\min}$ the desired molecular state $n = 4$ is reached almost perfectly. For simplicity, only the plots for the qubit channel $|11\rangle$ are shown here; the situation is very similar for the other channels. Note the different time scales used for the transport and phase-accumulation sequences, respectively.

and $|10\rangle$ states could also be effectively used for a SWAP gate, which inverts the populations of these two channels—or for its square root, which in combination with single-qubit rotations constitutes an alternative universal set of gates for quantum computation.

VI. CONCLUSIONS AND OUTLOOK

In this work we analyzed the spin-state-dependent interaction between a single atom and a single ion guided by external trapping potentials. We applied our insight on this system to realize a two-qubit quantum gate process and thereby provide the basic ingredients for quantum computation with atoms and ions combined in one setup. This work was motivated by recent experimental possibilities combining magneto-optical traps or optical lattices for atoms, and rf traps for ions. These experiments are currently established in several groups worldwide [8,17].

We started our description of controlled interaction of an atom and an ion by formulating an MQDT for trapped particles, analogous to the free-space case discussed in Ref. [9]. This step simplifies the description of atom-ion collisions because it does not require a detailed knowledge of the molecular potentials at short range. Experiments measuring the positions of Feshbach resonances can determine the two essential parameters for our theory—the singlet and triplet scattering lengths. Since these experiments have not yet been performed, here we focused on the case of similar singlet and triplet scattering lengths given in order of magnitude by R^*, whereas the general case of different scattering lengths was discussed only qualitatively.

We were able to reduce the multichannel formalism to an effective single-channel model that singles out a specific spin state of atom and ion. This model is found to be accurate for similar values of the singlet and triplet scattering lengths. In calculations we assumed $a_s = 0.9R^* = 4989a_0$ and $a_t = 0.95R^* = 5266a_0$ for the singlet and triplet scattering lengths, respectively. In contrast, opposite signs of scattering lengths exclude a single-channel description. We estimated the error introduced by our specific single-channel model to be 2×10^{-3}, which is due to a mixing of channels in the eigenstates of the system. Taking even closer values of singlet and triplet scattering lengths leads to better applicability of the single-channel description.

Where applicable, our effective single-channel model can be implemented in calculations in the context of ultracold chemistry as well as ultracold scattering physics. A single-channel description assigning quantum-defect parameters to each channel separately has already been discussed in Ref. [12]. However, the spin state was not included in previous research. In the present approach, starting from the fundamental parameters a_s and a_t of the multichannel formalism, we derive the quantum-defect parameters of each isolated channel consistently. We take the channel coupling into account and estimate the error introduced by assuming isolated channels. Therefore, the model can be applied to quantum computation schemes that store qubits in internal spin states of atom and ion.

A remarkable feature of the system is trap-induced shape resonances that couple molecular bound states to unbound trap states. Quasistatic eigenenergy curves show these resonances as avoided crossings. They can be used to form ultracold trapped molecular complexes and thereby allow full control of cold chemical reactions.

Trap-induced resonances also form the basis for our idea of the phase gate process. Initially an atom and an ion are prepared in the trap vibrational ground state. We realized a qubit-dependent two-particle phase via controlling the external degrees of freedom. By bringing the traps close together, we allowed the particles to interact and finally separated them, again obtaining the motional ground state. In doing so, we cross weaker resonances diabatically (remaining in a trap state) and then follow a stronger resonance adiabatically into a molecular bound state, where a two-qubit phase is accumulated. Since the positions of the resonances are different for each spin combination, the accumulated phase is different for each qubit channel and we are able to control the trap distance in such a way that a two-qubit phase gate

is realized. This phase gate, in combination with single-qubit rotations, is a universal gate for quantum computation.

We performed numerical simulations of the controlled collision specifically for a $^{135}Ba^{+}$ ion interacting with a ^{87}Rb atom, each guided by a spherically symmetric harmonic trap with $\omega_{i,a} = 2\pi \times 30$ kHz. Specific hyperfine qubit states were chosen to obtain the four qubit channels, 00, 01, 10, and 11. In this framework we developed a two-qubit phase gate process entangling an atom and an ion, thereby showing that trap-induced resonances can be used to control the atom-ion interaction. The error for our gate process is 1×10^{-3} and in this case the gate time is 1.3 ms. Using optimal control techniques we were able to accelerate the process to 346 μs. In future work we plan to decrease the gate time by using higher trapping frequencies to allow faster transport.

The choice of very similar scattering lengths allowed single-channel calculations to be performed, but it limits the gate time because the amount of energy splitting between the channels is rather small. A more general description can be done in the framework of our multichannel formalism, allowing for arbitrary combinations of singlet and triplet scattering lengths. It is possible that the actual values of the scattering lengths are in fact very different, which would require a more complicated multichannel computation but would possibly allow much faster quantum gates. However, in the regime considered here, a gate time of less than a millisecond ha already been demonstrated.

In our model, harmonic trapping potentials were assumed and the oscillator frequencies were equal for the atom and the ion. Among the advantages of ions for quantum computation is the existence of much tighter trapping potentials than those that exist for atoms. The basic ideas developed in this paper are expected to be applicable to more general situations with different trapping frequencies. A generalization is highly desirable, but it would lead to a more complicated theoretical treatment as, for example, c.m. motion becomes coupled to the relative motion. Very elongated cigar-shaped traps have already been treated in previous works. One of our goals is the consideration of particular experimental realizations in order to describe them with our theory, compare the results, or suggest directions of experimental research.

In the present, external magnetic fields were not used to manipulate the interaction. Magnetically induced Feshbach resonances have been applied very successfully to engineer neutral-atom collisions. Future investigations will include magnetic fields to control the atom-ion interaction even more efficiently and possibly combine trap-induced resonances and Feshbach resonances for this purpose. Our work can be seen as a principle investigation of an interesting physical system and can be extended in many directions.

ACKNOWLEDGMENTS

We acknowledge support by the European Union under the SCALA Integrated Project; the German Science Foundation through SFB TRR21 CO.CO.Mat; the National Science Foundation through a grant for the Institute for Theoretical Atomic, Molecular, and Optical Physics at Harvard University and the Smithsonian Astrophysical Observatory; and the Polish Government Research Grant. The authors would like to thank P. Zoller, P. Julienne, J. Hecker Denschlag, and P. Schmidt for fruitful discussions. H.D. thanks M. Trippenbach and the University of Warsaw for a very rewarding two-week visit.

[1] S. Bergamini, B. Darquié, M. Jones, L. Jacubowiez, A. Browaeys, and P. Grangier, J. Opt. Soc. Am. B **21**, 1889 (2004).
[2] Y. Miroshnychenko, W. Alt, I. Dotsenko, L. Frster, M. Khudaverdyan, D. Meschede, D. Schrader, and A. Rauschenbeutel, Nature **442**, 151 (2006).
[3] M. Greiner, O. Mandel, T. Esslinger, T. Hänsch, and I. Bloch, Nature **415**, 39 (2002).
[4] C.-S. Chuu, T. Strassel, B. Zhao, M. Koch, Y.-A. Chen, S. Chen, Z.-S. Yuan, J. Schmiedmayer, and J.-W. Pan, Phys. Rev. Lett. **101**, 120501 (2008).
[5] R. Dumke, M. Volk, T. Müther, F. B. J. Buchkremer, G. Birkl, and W. Ertmer, Phys. Rev. Lett. **89**, 097903 (2002).
[6] D. Leibfried, R. Blatt, C. Monroe, and D. Wineland, Rev. Mod. Phys. **75**, 281 (2003).
[7] W. W. Smith, O. P. Makarov, and J. Lin, J. Mod. Opt. **52**, 2253 (2005).
[8] A. T. Grier, M. Cetina, F. Oručević, and V. Vuletić, Phys. Rev. Lett. **102**, 223201 (2009).
[9] Z. Idziaszek, T. Calarco, P. S. Julienne, and A. Simoni, Phys. Rev. A **79**, 010702(R) (2009).
[10] Z. Idziaszek, T. Calarco, and P. Zoller (unpublished).
[11] O. P. Makarov, R. Côté, H. Michels, and W. W. Smith, Phys. Rev. A **67**, 042705 (2003).
[12] Z. Idziaszek, T. Calarco, and P. Zoller, Phys. Rev. A **76**, 033409 (16) (2007).
[13] T. Calarco, U. Dorner, P. S. Julienne, C. J. Williams, and P. Zoller, Phys. Rev. A **70**, 012306 (2004).
[14] M. Krych and Z. Idziaszek, Phys. Rev. A **80**, 022710 (2009).
[15] Y. Chen and B. Gao, Phys. Rev. A **75**, 053601 (2007).
[16] A. Barenco, D. Deutsch, A. Ekert, and R. Jozsa, Phys. Rev. Lett. **74**, 4083 (1995).
[17] S. Schmid, A. Härter, J. Hecker Denschlag, and A. Frisch (private communication).
[18] R. Stock, I. H. Deutsch, and E. L. Bolda, Phys. Rev. Lett. **91**, 183201 (2003).
[19] F. H. Mies, J. Chem. Phys. **80**, 2514 (1984).
[20] B. Gao, E. Tiesinga, C. J. Williams, and P. S. Julienne, Phys. Rev. A **72**, 042719 (2005).
[21] J. P. Burke, C. H. Greene, and J. L. Bohn, Phys. Rev. Lett. **81**, 3355 (1998).
[22] B. R. Johnson, J. Chem. Phys. **67**, 4086 (1977).
[23] T. Calarco, J. I. Cirac, and P. Zoller, Phys. Rev. A **63**, 062304 (2001).
[24] T. Calarco, E. A. Hinds, D. Jaksch, J. Schmiedmayer, J. I. Cirac, and P. Zoller, Phys. Rev. A **61**, 022304 (2000).
[25] W. H. Press, S. A. Teukolsky, W. T. Vetterling, and B. P. Flannery, *Numerical Recipes in C* (Cambridge University Press, Cambridge, England, 1992), 2nd ed.